Multi-diagnostic comparison of femtosecond and nanosecond pulsed laser plasmas

Z. Zhang,[a] P. A. VanRompay, J. A. Nees, and P. P. Pronko
Center for Ultrafast Optical Science and Department of Electrical Engineering and Computer Science, University of Michigan, Ann Arbor, Michigan 48109-2099

(Received 11 July 2001; accepted for publication 5 June 2002)

Understanding and fully characterizing highly dynamic and rapidly streaming laser ablation plasmas requires multiple techniques for monitoring effects at different stages. By combining multiple diagnostic methods, it is possible to analyze the broad time window over which these ablation plasmas develop and to learn more about the related physical processes that occur. Two laser sources, an 80 fs Ti:Sapphire laser (780 nm) and a 6 ns Nd:YAG laser (1.06 μm), are used in this work in order to compare pulse duration effects at similar wavelengths. Characteristics of the plasma produced by these two lasers are compared under conditions of comparable ablation flux. Results are presented involving correlation of time-resolved Langmuir probe data and electrostatic energy analysis for aluminum plasmas as a representative investigation for metallic systems. In addition, continuous-wave refractive index laser beam deflection is used to characterize the plasma and hot gas generated from boron nitride targets in terms of their ion and neutral atom densities. A self-similarity plasma expansion model is used to analyze the plumes under various conditions. Fundamental data obtained in this way can be relevant to laser micro-machining, laser induced breakdown spectroscopy, and pulsed laser deposition. © *2002 American Institute of Physics*. [DOI: 10.1063/1.1497449]

I. INTRODUCTION

This paper examines the fundamental physical properties of ablation plasmas generated by ultrafast and conventional nanosecond lasers having comparable wavelengths but 5 orders of magnitude difference in pulse duration. Comparisons are made for 100 femtosecond (fs) and 6 nanosecond (ns) pulsed-laser-plasmas formed with near-infrared laser irradiation. Several diagnostic techniques are used in this study to give a whole picture of the plasma development in terms of time and space. These methods, all of which are time resolved, include Langmuir probe, electrostatic ion energy analysis, and continuous wave (cw) laser beam deflection. Each technique investigates a different part or a different stage of the laser produced plasma. Irradiation intensities for the two laser ablation sources were chosen at the minimum level needed to give comparable signal intensity for each diagnostic being used. This form of comparison is necessary since the fs pulses have a significantly lower plasma breakdown threshold fluence, compared to ns pulses (at the near IR wavelengths being used), resulting in their ability to generate, in most cases, appreciable plasma intensity at comparably lower fluence levels. Comparing ns and fs plasmas at the same energy fluence would give misleading correlations due to the significant plasma threshold differences between them. In the case of the cw laser beam deflection, larger fluences are needed for the ultrafast pulses in order to generate comparable neutral fractions in the ablation plume. These fluence adjustments are, in and of themselves, interesting diagnostics in terms of how the two different laser pulses interact with the ablation target.

II. EXPERIMENTAL SETUP

The experiments were carried out in a stainless steel ultrahigh-vacuum chamber, which is turbo-molecular pumped. A base pressure of 5×10^{-9} Torr was reached with an internal liquid nitrogen cryotrap in place. Background gas can be introduced, if needed, into the chamber through a precision metal leak-valve. The ablation-target manipulator holds four 1 in. targets with full individual rotation and selective clocking motion. Rotation and rastering allow for uniform removal of target material with successive laser shots. Langmuir probe, optical emission spectrometer, electrostatic energy analyzer, and HeNe deflection probe are attached to the chamber as depicted in Fig. 1. Optical emission data will not be presented here but will be part of a different report. The temporal and spatial development of laser-produced plasmas and their composition are studied, in the present work, by a combination of these techniques. Typical error bars for the various data sets are shown in the appropriate data presentation figures.

The ultrafast laser used in this work is a 10 Hz, Ti:Sapphire, chirped-pulse amplified system producing pulses with energy up to 60 mJ, and with pulse width of 60 to 150 fs at a wavelength of 780 nm in *s*-polarization. Data from this laser is compared to results from a commercial Nd:YAG laser with a pulse width of 6 ns and a comparable wavelength of 1.06 μm. The energy of the fs laser output can be adjusted using a polarizer positioned before the compressor gratings.

[a]Electronic mail: zhiyuz@umich.edu

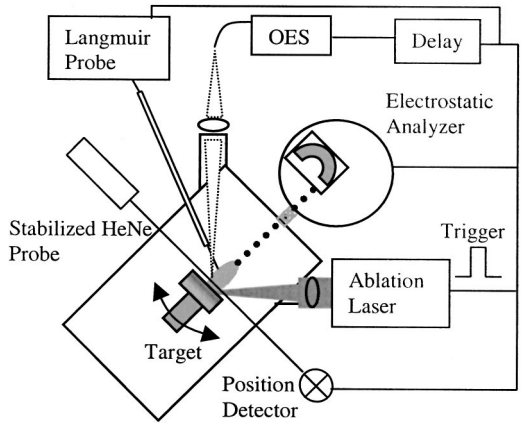

FIG. 1. Apparatus for laser produced plasma diagnostics including Langmuir probe, optical emission spectrometer, electrostatic analyzer, and HeNe deflection probe.

A 75 cm focal length lens was placed on a translation stage to allow variation of the laser spot size at the target. Both laser beams were focused, with this lens, on the target at an angle of 45° relative to the target normal.

In the present work, a classical electrically scanned Langmuir probe is used to study plasma characteristics. Simple, nonvoltage scanned, time-of-flight ion probes have been widely used to study laser-ablation plumes. These usually consist of a wire extending into the plasma with plasma current read out to an oscilloscope. Such probes are often biased at a negative voltage and used to collect the ion time-of-flight signal from an ablation plume. However, a recent study[1] showed that this method might not accurately detect the correct ionic component in the plume because of secondary electron generation dominating the ion probe signal. In the present work, the probe is scanned in negative and positive voltage with the current–voltage response properties being used to obtain detailed information about the plasma. Extensive probe theories[2] have been developed to extract electron temperature T_e, electron and ion density (N_e and N_i), plasma potential V_p, and plasma floating potential V_f from such I–V curves. The Langmuir probe we used[3] was installed on the chamber through a bellows adapter, which provides the ability to spatially locate the probe and thereby achieve both spatial (3 mm) and temporal (1 μs) resolution of the plasma parameters. The timing of probe data acquisition is controlled using a programmable delay/pulse generator triggered by the laser signal, so that temporally resolved plume diagnostics can be achieved. In order to increase the signal-to-noise level, each data point was averaged over 20 laser shots. The probe is typically biased from -15 to $+20$ V over a 1 μs time interval.

A spherical-sector, electrostatic energy analyzer is connected to the main chamber to provide a detailed study of the ion and neutral species in the ablation plume. Two microchannel plate (MCP) detectors are mounted on the energy analyzer, one on the curved sector for comprehensive charged particle analysis, and the other on the straight-through port for high-energy neutral ($>$100 eV) or total (including low energy) ion count. The distance from target surface to the energy-analyzing detector is 110 cm. The energy analyzer selects ions with a particular energy-to-charge ratio (E/q). Particles with the same E/q but different charge will have different velocities and will arrive at the analyzer MCP at different times. Coupled with time-of-flight analysis and with a scanning voltage on the sector plates, the energy analyzer can map out the entire energy, charge-state, and ionic mass distribution of the ablation plume. The output signal from the MCP can be converted to ion current density for each charge state if the efficiency of the MCP is taken into account. Ion current density divided by the ion velocities obtained from the kinetic energy gives the ion volume density. After adding the ion volume density for different charge states together, a comparison can be made of the total ion density at the MCP detector to the ion density given by the Langmuir probe.

Knowing properties of the neutral component in a laser-generated plume is an important part of characterizing the ablation process. The ion and electron diagnostic methods discussed above are unable to study the medium and low energy (1 eV$<E<$100 eV) neutral component in a direct fashion. To accomplish this, a stabilized HeNe laser beam is used as a transverse probe of the plume. In general, the neutral component of the plume has an order of magnitude slower mean velocity than the plasma component. These temporally separated ionic and neutral components in the plume deflect the probe beam in opposite directions due to their radically different refractive indices.[4] The deflection is detected and recorded by a segmented fast photo detector. The number of ion and neutral atoms in the plume can then be extracted from the deflection data. Further discussion of this method is presented in Sec. III D below.

III. RESULTS AND DISCUSSION

A. Langmuir Probe Results

The time resolved Langmuir probe tip was placed, on axis, either at 5 or 10 cm away from the ablation target surface, with a typical growth substrate holder in its normal position (near 10 cm) and grounded. This provides two grounded surfaces between which the plasma travels. The probe obtains an experimental I–V curve in a 1 μs time interval. Similar curves are sample-averaged over multiple laser shots. Analysis of the sample-averaged curve provides electron and ion densities and electron temperature as a standard output of the data. Other parameters of the plasma are readily calculated from these.[2]

In Figs. 2(a) and 2(b) are presented time-resolved data from the probe for 100 fs and 6 ns ablation plasmas from an Al target. Some interesting comparisons can be made between these two experimental conditions. There are both differences and similarities between the two cases. It is seen that for the conditions of the observations, the ion and electron densities are similar for both ns and fs pulses. These levels are a consequence of the laser fluences chosen for the experiment. In both cases, the measured ion densities are seen to be slightly larger than the electron densities. This may be an artifact due to secondary electron emission during the ion portion of the measuring cycle or inadequate ground path for the plasma current. The latter is not thought to be the

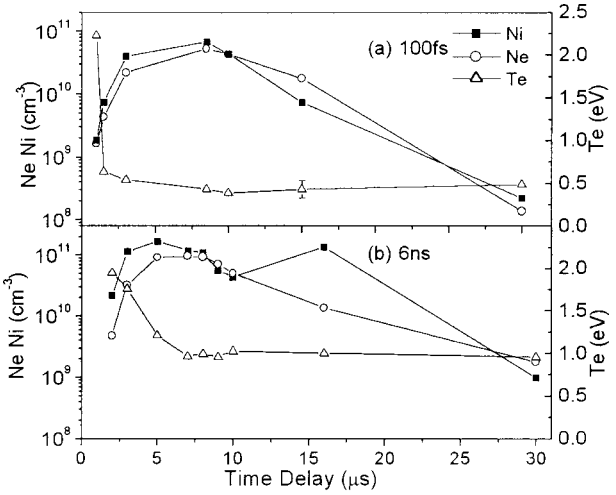

FIG. 2. Ion density, electron density, and electron temperature of an Al ablation plume produced by (a) 100 fs, 780 nm laser pulses with energy fluence of 0.4 J/cm^2 and (b) 6 ns, 1.06 μm laser pulses with energy fluence of 1.3 J/cm^2. The probe was placed at 10 cm away from the Al target surface.

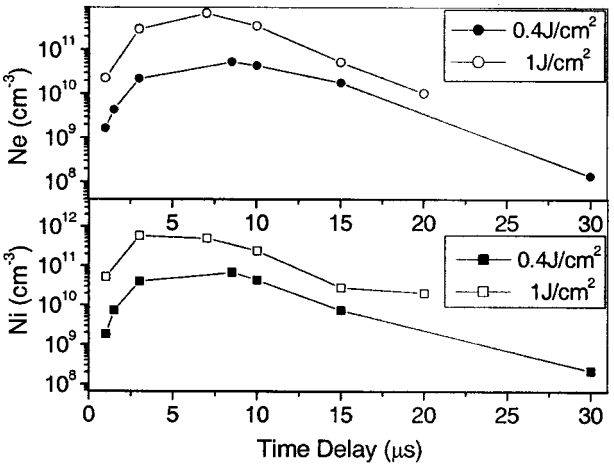

FIG. 3. Electron and ion density of ablation plumes produced by 100 fs, 780 nm laser pulses with fluence of 0.4 J/cm^2 and 1 J/cm^2 respectively. The probe is placed at 10 cm away from an Al target surface.

case since the grounded substrate holder is immediately adjacent to the probe. On the other hand, it might indeed be a legitimate imbalance between N_i and N_e where the streaming plasma is only quasineutral. In laser-induced plasma formation, the electrons absorb the laser energy first and begin to expand ahead of the ions. The space-charge effects from this separation could induce consequences (such as return of electrons to the laser target) that result in the observed charge imbalance seen in Figs. 2(a) and 2(b). The launching of hot electrons ahead of the main body of the plume is clearly seen in the temporal dependence of the electron temperature for both fs and ns cases as shown in the figure. For the ns case, the high-temperature electrons mix into the first 15%–20% of the main body of the plume. It is observed however that the leading edge of the fs plume has a much thinner hot-electron section than the ns case. In addition, the electron temperature (right side of Fig. 2) in the ns case remains about a factor of 2 higher across the entire plume compared to the fs case. It is probable that these results are a consequence of the additional plasma heating that occurs for the 6 ns pulse. The difference here is related to the fact that fs plasmas can form due to electric field excitation of the plasma at the surface[5] instead of direct bulk heating, which predominates under ns irradiation.[6] In addition, plasma heating during expansion occurs due to the longer time duration of the ns pulse. In the fs case, the hot electrons are only associated with the very highest energy ions in the plume, they being a factor of approximately 50 to 100 less in concentration compared to ions in the main body of the plasma plume.

B. Ion–electron plasmas

In this section, we examine correlated information obtained from ion and electron densities and electron temperatures as they are obtained from the Langmuir probe as a function of laser fluence. In Figs. 3 and 4 are shown ion- and electron-density data obtained with the Langmuir probe for fs pulses as a function of laser intensity and distance from an aluminum ablation target. It is observed in Fig. 3, where both ion and electron densities are presented as a function of delay time, that an interesting nonlinear behavior exists between these densities and the laser ablation fluence. These data are for 100 fs pulses at 780 nm. Increasing the laser fluence by a factor of 2.5 (from 0.4 to 1.0 J/cm^2) results in an increase of the ion and electron densities near a simulated deposition substrate by factors of 10 or more depending on time. Normally growth rates increase either linearly or sublinearly with laser fluence. This suggests that the ion densities increase, in the present case, at the expense of excited and/or ground state neutral atoms in the plume. Controlling the concentration of ions, and their kinetic energies, in relation to the neutral atoms in the plume could be an important parameter for certain types of applications such as film growth.

Figure 4 illustrates how the 0.4 J/cm^2 plasma changes its ionic density in the region between 5 and 10 cm. At 5 cm, the high-velocity ionic component of the plume is seen to be

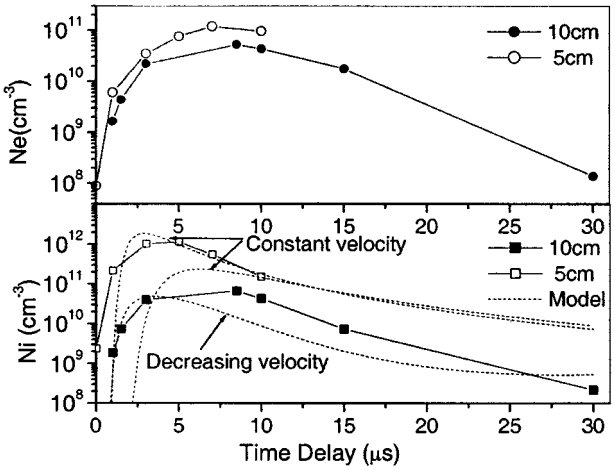

FIG. 4. Electron and ion density of ablation plumes produced by 100 fs, 780 nm laser pulses with a fluence of 0.4 J/cm^2. The probe is placed at 5 and 10 cm away from an Al target surface respectively. The results of a self-similar expansion model for the ions are also shown.

significantly higher than and out of balance with the electron densities, the difference being more than one order of magnitude. However, by the time the plume reaches 10 cm its ionic concentration has diminished by more than a factor of 20. At this point, the ionic component is close to being in balance with the electron densities, whose volume concentration has decreased by only a factor of 4 in the final 5 cm distance. The process by which this occurs is related in some way to the expansion physics of the ionic component and its achieving quasineutrality over that final 5 cm to the substrate. Balancing of space charge in the plasma, across that final distance to the substrate, is more likely a consequence of the ionic component of the plasma enlarging its occupied volume to more nearly match the electronic spatial distribution in the intervening space. For simple hemispherical radial expansion, the detected volume concentration of ions, based on detector solid angle considerations, should decrease approximately as $1/R^2$, where R is the distance from the ablation source. Examination of the change in ion densities in Fig. 4 shows that the high-velocity component decreases somewhat more rapidly than predicted by a $1/R^2$ dependence. The distance changes by a factor of 2, whereas the ion concentrations change by more than an order of magnitude. This concentration change should be a factor of 4 if geometry were the only consideration. These observations suggest that more than simple radial expansion of the ionic component of the plume is occurring over distances involved in Fig. 4. If one examines the change in electron densities across the intervening distance, it is seen that they drop less rapidly than expected from geometric considerations alone, thus further confirming the difference in expansion behavior between the ions and electrons.

Use of a self-similarity model can provide more detailed analysis of expansion for the hydrodynamic component of a laser-produced plasma. The concept of self-similar solutions for gas dynamics problems is described in detail by Zel'dovich and Raizer.[7] A general derivation, from hydrodynamic equations, is given by Hora[8] showing how a self-similar expansion for a laser plasma evolves from a flat surface. For such a case, the model provides velocity and density distributions given as

$$v(r,t)=v(t)(r/R). \tag{1}$$

In Eq. (1) the individual ion velocity profile in the plasma is a linearly increasing function of distance from the surface, r, out to some maximum value R. The density distribution is given as

$$n_i(r,t)=(n_0/\pi^{3/2}l^3)\exp(-r^2/l^2), \tag{2}$$

where n_0 is the total number of ions in the plasma. This distribution has a characteristic Gaussian form that is parametrized by the quantity l, which is considered to be a function of time only. In the case of expansion from a flat surface the equations can be further generalized into coordinates of expansion normal to the surface and at right angles to it.[9] Such details are addressed in Sec. III D where hydrodynamic expansion is given further consideration. For the purposes of this section Eqs. (1) and (2) are sufficient. Considering the z component of the expansion (normal to the ablating surface), Eq. (2) is given in terms of the distance and time. The quantity l is normally given as v_0t, where v_0 is a characteristic group expansion velocity for the Gaussian profile as a whole. In the simplest case, v_0 is a constant. Our results for the ionic component at the 5 cm position in Fig. 4 are reasonably consistent with this and yield a v_0 value of $(1.42\pm0.43)\times10^6$ cm/s over the 10 μs time interval measured. The results of fitting Eq. (2) using this value for v_0 are shown in the figure. If the same constant expansion velocity is used for the 10 cm case, it is seen that the model predicts a higher ionic density than is observed experimentally. We find that, in order to fit the model to the 10 cm case, it is necessary to use a v_0 that is a decreasing function of time and takes on the empirical form of $v_0=a\exp[b/(t+c)]$, where $a=2.83\times10^4$ cm/s, $b=51.38$, and $c=9.97$, and t is in units of microseconds. Using this time dependent function for v_0 in the $l=v_0t$ form provides a fit to our observed 10 cm data as seen in Fig. 4. Using this fitting equation, the expansion velocity at 3 μs is 1.48×10^6 cm/s, whereas it is 2.21×10^5 cm/s at 15 μs. The fact that v_0 is constant at 5 cm and a rather strong decreasing function of time at 10 cm suggests that a significantly different physical condition for the plasma occurs between 5 and 10 cm. The implication is that over the intervening distance the plasma has given up internal energy that is no longer available for driving the adiabatic expansion process described by the self-similar solution. This loss of internal energy can be from radiation or some other form of energy dissipation unique to the electrodynamic expansion of the plasma. This result suggests that the distance from an ablating target to a growing substrate is an important parameter when growing thin films by such ultrafast pulsed-laser deposition.

C. Ion energy analysis

The spherical-sector ion energy analyzer is a sensitive device that can measure the energy distributions of individual ionic charge states within the ablation plasma. It very clearly demonstrates that there are two distinct ion populations in the plasma plumes. These can be distinguished as a hydrodynamic component and an accelerated component. The accelerated ions come from a combination of ambipolar field effects,[10] Coulomb explosion, and nonlinear pondermotive forces.[11] The hydrodynamic component is similar for both the ns and fs laser pulsed plasmas. However, the accelerated component is always more pronounced for the fs case. Indications of these effects are visible in the data of Figs. 5 and 6 where ion signals are shown at the analyzer in terms of ion energy density functions. The hydrodynamic component of the plasma is observed in an energy region on the order of or less than 100 eV, whereas the accelerated component extends to energies above that range. It is seen in Fig. 5(a) that the vacuum ion signal from 6 ns pulses consists predominantly of low energy ions in the hydrodynamic range. Charge states 1 and 2 are observed. This is to be compared to Fig. 5(b) in which 80 fs ion yields are shown. In this case, charge states 1, 2, and 3 are present in the form of a high-energy component in addition to the low-energy, charge-state 1 component. In Fig. 6 are seen the effects of 0.8 mTorr back-

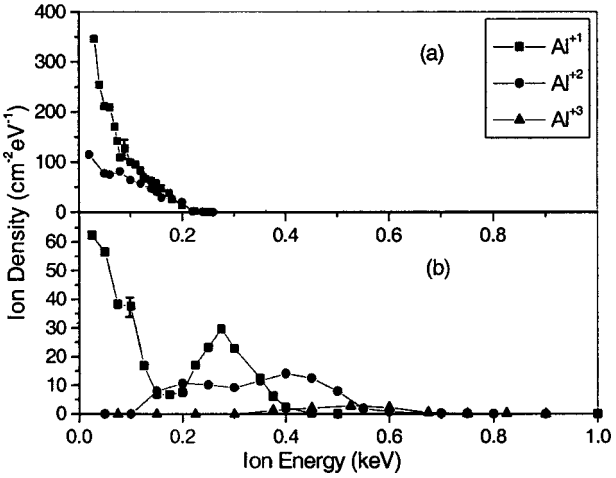

FIG. 5. Ion-energy spectrum for Al ablation in vacuum by (a) 6 ns laser pulses at 1.06 8μm with energy fluence of 1.3 J/cm^2 and (b) 100 fs laser pulses at 780 nm with an energy fluence of 0.4 J/cm^2. Note the change in scale on vertical axis for the two conditions.

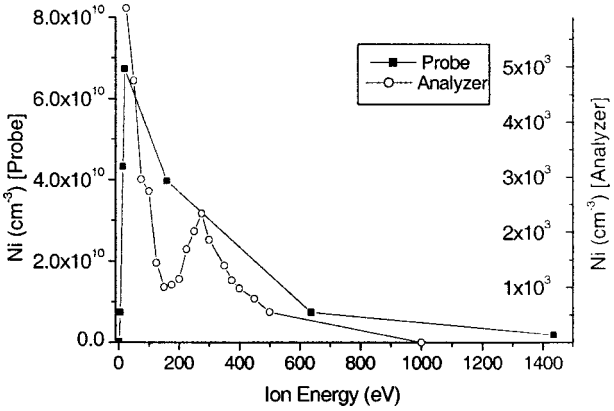

FIG. 7. Ion-energy distribution for Al ablation in vacuum from Langmuir probe and ion-energy analyzer for 100 fs, 780 nm, 0.4 J/cm^2 laser pulses are used in both cases. The data for the probe and analyzer are plotted on different vertical axes. The probe is located at 10 cm, the analyzer at 110 cm.

ground gas being introduced into the chamber with no gas discharge occurring. The presence of the gas causes the higher charge states to convert, by charge exchange, to mostly charge-state 1 with only a small component of charge state 2 being left. The background gas can be made to discharge by applying high voltage (+1300 V) to an annular ring placed at about 6 cm from the ablation target. When this is done the charge exchange process is further augmented; however, here the low-energy part of the spectrum is most affected. In this case, a significant percentage of the low-energy charge-state 1 is converted to excited or ground state neutrals. Only a small percentage of the higher-energy portion of charge-state 1 is seen to remain. Thus, the presence of the discharge gas greatly modifies the ion-energy densities in the deposition plasma, producing a highly moderated and atomically activated form of the initial ablation plume, which becomes mixed with the activated background gas. Such conditions are often used for growing multi-component films by the pulsed laser deposition (PLD) method.

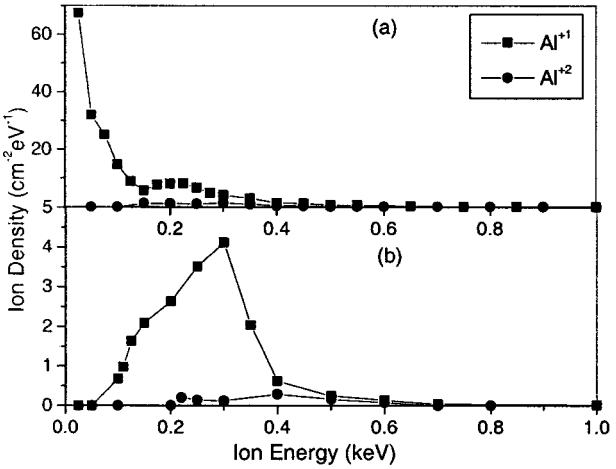

FIG. 6. Ion-energy spectrum for Al ablation plume produced by 100 fs laser pulses at 780 nm with energy fluence of 0.4 J/cm^2. (a) 0.8 mTorr N_2 background gas only, (b) 0.8 mTorr N_2 background gas and discharge. Note the change in scale on vertical axis for the two conditions.

Interesting correlations can be made for the ion-energy distributions in the ablation plasmas by comparing the Langmuir probe results with those from the ion-energy analyzer. This is done in Fig. 7 where the ion density from the Langmuir probe is now plotted as a function of kinetic energy. This is obtained by converting from time delay, at a particular distance, to ion velocity and subsequently to ion kinetic energy. These ion densities as a function of energy are compared to similar data obtained directly from the ion-energy analyzer as described in the experimental section. Data in Fig. 7 is presented for 80 fs pulses at 0.4 J/cm^2 for both the probe and the analyzer. It is seen in the figure that the two curves are similar in general appearance but with the energy analyzer showing more detail than the ion probe. The significance of this comparison is that the ion-density signal obtained with the energy analyzer can now be calibrated directly against the Langmuir probe. As such, it can then be used to infer highly detailed information about the ion concentrations as a function of energy, charge state, and even isotope ratio at an intermediate distance from the ablation target, where for example thin films might be grown. The difference in the absolute ion densities seen by the probe and the analyzer is determined by their large difference in distance from the ablation target (110 versus 10 cm).

D. Hydrodynamic neutral and ionic component by refractive index

In this section, we investigate the neutral component in the laser-produced plasma using a cw HeNe probe laser passing transversely across the plume (see Fig. 1). Since the ion-to-neutral ratio is often critical in the formation of certain thin film phases, such as cubic boron nitride (c-BN), we studied a boron nitride target for this part of the experiments. Figure 8 shows a typical HeNe probe time-resolved deflection signal recorded by a position sensitive photodetector. The plume, for that case, was produced with 6 ns pulses at 1.06 μm using a fluence of 18 J/cm^2. The probe laser beam

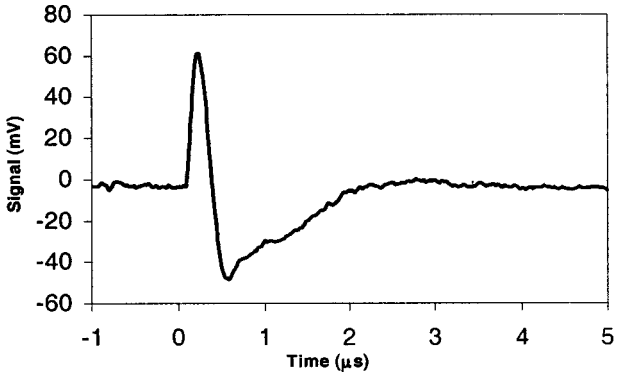

FIG. 8. A typical laser deflection signal. The plume was produced by 6 ns, 1.06 μm, 100 mJ pulses from a BN target. The positive peak is from the plasma deflection and the negative peak from the neutral particles.

was 2 mm away and parallel to the target surface. As per discussions by Enloe *et al.*[4] deflection is caused by the index gradient, normal to the target surface, of electrons in the plasma and neutral atoms in the plume. The ion–electron plasma typically travels faster than the neutrals and is therefore detected earlier. The index gradient of neutral particles is positive; therefore, the probe beam is deflected toward the target surface giving a negative signal for the detector setup used in this experiment. On the other hand, the index gradient of the plasma is negative, producing a positive signal for the ions since the beam is deflected away from the target. The refractive index of the plasma is a function of its free electron density. It is assumed here that the ion/electron ratio is unity. This may or may not be the case depending on details of the streaming plasma balance as discussed in Sec. III A. These ion-to-neutral ratios will therefore represent lower limits. Since the change in the index of refraction of both plasma and neutral particles is proportional to its corresponding density, the deflection amplitude can be related to the total number of ions or neutral atoms, under a self-similar expansion model,[4,9] using Eqs. (3) and (4),

$$|\phi_{\text{plasma}}|_{\max} = 1.24\times 10^{-22}\frac{Z_{\text{eff}}N_{\text{Ti}}k_i^3}{Z^3}, \tag{3}$$

$$|\phi_{\text{neutral}}|_{\max} = 7.08\times 10^{-24}\frac{N_{\text{Tn}}k_n^3}{Z^3}. \tag{4}$$

Here ϕ is the deflection angle, Z_{eff} is the effective ionic plasma charge, N_{Ti} and N_{Tn} are the total number of the ions and neutral atoms produced by the laser shot, Z is distance from probe to the target surface, and k_i and k_n are the ratios of the longitudinal and radial velocities of the i and n components, respectively.

The peak density of each component along the path of the probe laser can be calculated from the self-similar expansion model using Eqs. (6) and (11) from Ref. 4 and is given by Eq. (5)

$$n_j = \frac{2N_{Tj}k_j^2}{\pi^{3/2}(Z/\sqrt{2})^3}\exp(-2); \quad j=i \text{ or } n. \tag{5}$$

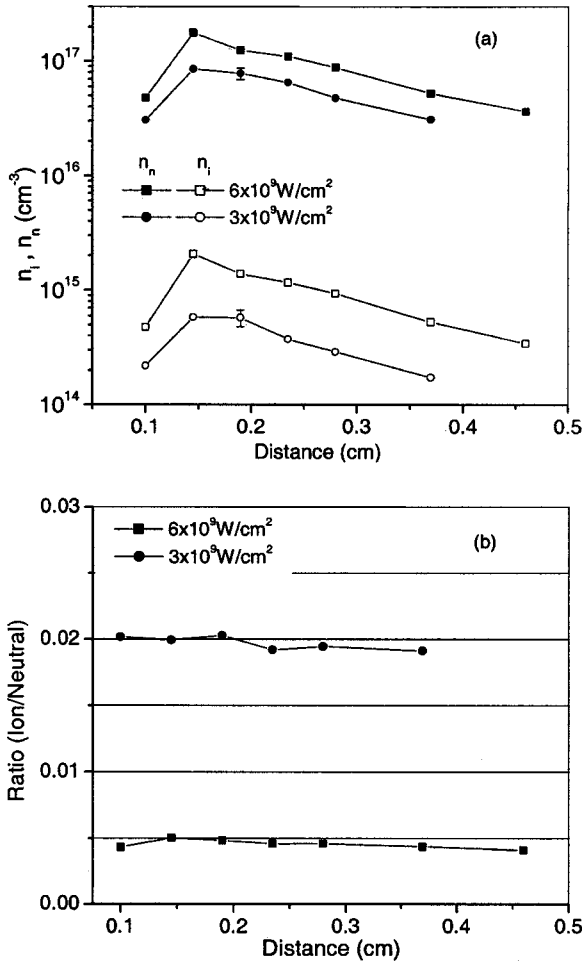

FIG. 9. Ion density and neutral particle density (a) and ion-to-neutral ratio (b) in plumes produced by 6 ns, 1.06 μm pulses at an intensity of 6×10^9 W/cm^2 (36 J/cm^2) and 3×10^9 W/cm^2 (18 J/cm^2).

Moving the target relative to the probe beam can change the distance between the probe beam and target surface. Systematic peak shifting can be observed as the probe distance from the target surface is increased. The velocity of ions and neutrals can therefore be extracted from the distance and associated peak delay. Using this method, the velocity of the ion–electron plasma generated with 6 ns pulses at 6 J/cm^2 is found to be 5.7×10^6 cm/s whereas for the 160 fs pulses at 1.1 kJ/cm^2 it is 3.7×10^6 cm/s, the fluence in the latter case being considerably higher to achieve comparable ion velocities. The neutral particles have a velocity of 0.8×10^6 cm/s for both cases, which corresponds to a most probable neutral kinetic energy of 4 eV. The most probable velocity for the ions corresponds to energy of 190 and 85 eV for the ns and fs cases, respectively. Compared with the ion energy distribution obtained using the ion energy analyzer in Fig. 5, we found that the energy range that the HeNe probe detects does not include the characteristic high-energy ions as are always observed in a fs energy distribution.[10] These high-energy ions are of relatively low concentration compared to the more predominant hydrodynamic ions, the latter being the component that is detected by the HeNe probe. Figures 9 and 10 show the ion and neutral density and the ratio of the number of ions to neutral atoms in a boron nitride plume

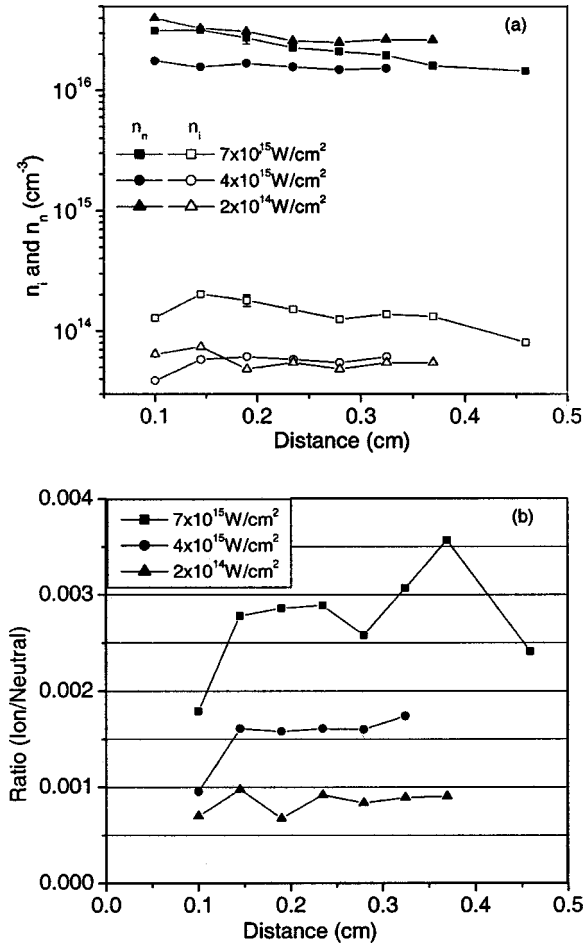

FIG. 10. Ion density and neutral particles density (a) and ion-to-neutral ratio (b) in the plume produced by 160 fs, 780 nm pulses at intensities of 7×10^{15} W/cm^2 (1.1 kJ/cm^2), 4×10^{15} W/cm^2 (0.64 kJ/cm^2, by reducing the energy), and 2×10^{14} W/cm^2 (32 J/cm^2, by increasing the focal spot) respectively.

produced by the 6 ns pulse and 160 fs pulse respectively. The ion to neutral ratios are similar to that observed for carbon ablation in vacuum, as reported in Ref. 4 using a similar technique; however, these ratios are significantly lower than reported in Ref. 12 for silicon ablated in air and analyzed through the Saha equation.

The intensities for the 6 ns data in Fig. 9 are 3×10^9 W/cm^2 (18 J/cm^2) and 6×10^9 W/cm^3 (36 J/cm^2), as obtained by varying the pulses energy from 100 to 200 mJ. In the case for 160 fs pulses (Fig. 10), both the laser focus spot size and energy were varied to change the intensity. In that case, the highest intensity of 7×10^{15} W/cm^2 (1.1 kJ/cm^2) was reduced by approximately a factor of 2 with energy to 4×10^{15} W/cm^2 (0.6 kJ/cm^2) and a factor of 35 with spot size to 2×10^{14} W/cm^2 (spot diameter of 71 μm increased to 434 μm). The ion density in the plume produced by 6 ns pulses is nominally one order of magnitude higher than that produced by the 160 fs pulse, similar to what is seen for the hydrodynamic component in Fig. 5. The neutral density is only a factor of 3 higher although the laser intensities are five orders of magnitude apart. Similarly as shown in Fig. 10(a), although the intensity was decreased by a factor of 35 by varying the 160 fs laser focus spot, the density of neutral particles does not show a dramatic change. Within the limited amount of data available here, the quantity of material ablated from the target, which is dominated by the neutral particles, appears to be less sensitive to the laser intensity (by varying the spot size or the pulse width) and rather more sensitive to the energy of the pulse. However, the ion-to-neutral ratio can be changed by the laser intensity as shown in Fig. 10(b). It is also noted that the ratio can be increased more efficiently (in terms of the intensity) by varying the energy of fs pulses rather than spot size. The ion-to-neutral ratio of the plume generated by 6 ns pulses is increased by approximately 2 as the energy of the pulse is doubled. A similar effect is seen for the 160 fs case as well. On the other hand, the largest ion-to-neutral ratio in the 160 fs pulse ablated plume is 1 to 400 for the highest energy and tight focus case. This ratio is three times larger than the one produced by pulses with 1.7 times lower energy. The kinetic energy of the ions in Fig. 10 is 49 and 15 eV for the lower energy and larger spot size ablation compared to the 85 eV for the high energy and tight focus case. This demonstrates a convenient way to adjust the mean hydrodynamic ion energy of the plumes.

IV. CONCLUSIONS

We have demonstrated various diagnostic techniques that can be used to analyze pulsed laser ablation plumes and the correlations that exist between them for nanosecond and femtosecond laser pulses. The generation and expansion of pulsed laser plasmas is a relatively complex process, since, for example, the plasma density can be as high as solid density when it is created on the target surface and as low as 10^{11} cm^{-3} at a distance where, for example, a thin film is deposited. Knowing properties of the early stage high-density plasma is potentially relevant to understanding mass transport phenomena such as internal chemical segregation or isotopic enrichment. Additionally, properties of the neutral component in the ablation plume are important since the neutral component dominates the incoming flux on a film growth substrate. It is useful to characterize therefore the spatial and temporal properties of an expanding ablation plume by a variety of methods, each being unique to a particular stage of plume expansion and to correlate these results into a single comprehensive picture. The work presented here represents steps in that direction. Applications of these methods to the characteristics of grown films are underway and will be presented as a separate report.

Specifically, the electrostatic ion energy analyzer detects various ionic components in the ablation plume and provides energy distributions for specific charge states. Although the detector is located typically far from the ablation target, the measured ion energy distributions are a result of early stage interactions between charged particles and the built-in bipolar electrostatic field, which exists very near the target surface. The plasma retains these attributes and carries them into the low plasma density regime as a result of rapid adiabatic expansion. In similar fashion, the Langmuir probe detects the integrated ion component of the plasma; however, it provides temporal and spatial information for the ion and electron densities and plasma temperature. More signifi-

cantly, it measures these properties in the spatial zone intermediate between the ablation target and the ion energy analyzer. This provides, for example, a very direct mechanism to correlate the characteristics of an ablation plume with the characteristics of PLD thin films. The neutral component of the ablation plume can be analyzed using a low-power continuous HeNe laser beam, which is spatially deflected by the refractive indices of the ablation plume components. However, the density gradients required to get a strong deflection signal are rather high so that relatively high-intensity laser ablation beams are applied to generate such plasmas. Therefore, the data extracted from HeNe deflection measurement represents a more extreme condition compared to the probe and analyzer. It should also be noted that the ionic component seen by this technique is the high concentration, low energy hydrodynamic component, of the plume.

In this paper, we compared nanosecond and femtosecond laser ablation plumes using pulse energies that provide similar diagnostic signal strengths and potential thin film growth rates. Under such circumstances, it is observed that the ns pulses produce a greater concentration of low energy and low charge-state ions compared to the fs case. The fs pulses produce well-defined plasmas at lower energy fluences than the ns case and are more efficient at producing high-charge-state and high-energy ions. Long pulse heating of the plasma was identified as being responsible for higher electron temperatures in plasmas generated by ns pulses. For ns and fs pulses, the neutral component represents a significantly larger percentage of the ablation plume flux in comparison to the plasma component. However, it has much lower kinetic energy than all of the observed ionic species in the plasma components.

[1] J. C. S. Kools, S. H. Brongersma, E. van de Riet, and J. Dieleman, Appl. Phys. B: Lasers Opt. **53**, 125 (1991).
[2] N. Hershkowitz, in *Plasma Diagnostics*, edited by O. Auciello, D. L. Flamm (Academic, Boston, 1989), Chap. 3, and references cited therein.
[3] Scientific Systems, Inc.
[4] C. L. Enloe, R. M. Gilgenbach, and J. S. Meachum, Rev. Sci. Instrum. **58**, 1597 (1987).
[5] P. P. Pronko, P. A. VanRompay, C. Horvath, F. Loesel, T. Juhasz, X. Liu, and G. Mourou, Phys. Rev. B **58**, 2387 (1998).
[6] P. P. Pronko, S. K. Dutta, D. Du, and R. K. Singh, J. Appl. Phys. **78**, 6233 (1995).
[7] Ya. B. Zel'dovich and Yu. P. Raizer, *Physics of Shock Waves and High-Temperature Hydrodynamic Phenomena*, Vol. II (Academic, New York, 1966), Chap. XII.
[8] H. Hora, in *Laser Interaction and Related Plasma Phenomena*, edited by H. J. Schwarz and H. Hora (Plenum, New York, 1971), Chap. 4, p. 365.
[9] G. J. Tallents, Laser Part. Beams **1**, 171 (1983).
[10] P. A. VanRompay, M. Nantel, P. P. Pronko, Appl. Surf. Sci. **127–129**, 127 (2000).
[11] H. Hora, in *Laser Plasma Physics—Forces and The Nonlinearity Principle* (SPIE, Bellingham, WA, 2000).
[12] H. C. Liu, X. L. Mao, J. H. Yoo, and R. E. Russo, Spectrochim. Acta, Part B **54**, 1607 (1999).